Resonant First- and Second-Order Raman Scattering in GaP

B. A. Weinstein* and Manuel Cardona
Max-Planck-Institut für Festkörperforschung, Stuttgart, Bundesrepublik Deutschland
(Received 30 March 1973)

The dependence on laser frequency of the scattering cross section for allowed and forbidden first-order Raman scattering and for second-order scattering is presented. The measurements were performed in the vicinity of the E_0 and $E_0 + \Delta_0$ gaps. It is shown that the Γ_{15} components of the Raman tensor exhibit a sharp resonance at E_0 while Γ_1 components resonate both at E_0 and $E_0 + \Delta_0$. The results are interpreted in terms of a theory which assumes parabolic bands extending to infinity. The second-order scattering is produced mainly by electron–two-phonon interaction vertices, except for the strongly resonant sharp peaks which correspond to the creation of two LO phonons with $\vec{k} \simeq 0$ (Γ_1) and one LO plus one TO phonon with $\vec{k} \simeq 0$ (Γ_{15}). From these measurements, values for the electron–two-phonon deformation potentials are obtained.

I. INTRODUCTION

First-order Raman scattering measurements give only information about phonon states with $\vec{k} \simeq 0$. This severe limitation can be overcome by using the second-order Raman spectra: Two phonons with $\vec{k}_1 + \vec{k}_2 \simeq 0$ are then produced and the complete phonon spectrum becomes accessible. The various irreducible components of the second-order Raman spectra are related to combined densities of two-phonon states multiplied by the appropriate scattering probabilities, i.e., the corresponding squared matrix elements of the polarizability tensor. It is, therefore, in general very difficult to extract from the observed spectra information about individual phonons. Thus, the inverse path is usually followed: The various components of the Raman tensor are calculated from the phonon spectra obtained with neutron scattering by the use of lattice dynamical models (shell model) which include nonlinear interactions. This procedure has been successfully used for the alkali halides[1] and for MgO.[2]

In contrast to the rocksalt-structure materials,[3,4] the second-order Raman spectra of the tetrahedral semiconductors appear to be quite simple.[5–8] The completely symmetric (Γ_1) component of these spectra is produced mainly by phonon overtones (two phonons of the same frequency and opposite $\vec{k}$) and gives a rather undistorted picture of the corresponding density of one-phonon states (with the frequency scale expanded by a factor of 2) since the scattering probability varies gradually through it. The Γ_{15} component, smaller in intensity than the Γ_1, represents mainly combination scattering (two phonons belonging to different branches). The Γ_{12} component is nearly negligible. In this paper we present the variation of the cross section for the Γ_1 and Γ_{15} components of the two-phonon Raman spectra of GaP as a function of the frequency of the scattering radiation in the region around the direct band gap ($E_0 = 2.78$ eV at room temperature). This material was chosen instead of Ge, the family prototype, because its E_0 gap is accessible to available lasers (other possible choices, such as ZnTe, ZnSe, and AlSb will be the object of future work.) It is shown that most of the GaP spectrum resonates when approaching E_0 in a manner similar to the allowed one-phonon scattering. From this fact, and from theoretical considerations, we reach the conclusion that the second-order process is produced mainly by the electron–two-phonon interaction in first order with the electron–two-phonon vertex renormalized so as to include most of the electron–one-phonon processes taken in second order. Values of the corresponding electron–two-phonon deformation potentials D_1 and D_{15} are obtained.

Very little work on the photon energy dependence of the second-order Raman cross section has so far appeared. This is due to the fact that most materials studied (alkali halides,[3] alkaline earth chalcogenides[4]) have very large band gaps, not accessible to available lasers. Some indication of resonant behavior in the second-order Raman spectrum has been reported for TlBr.[9] In the case of semiconductors, with accessible gaps, work of a qualitative nature has been performed for the overtones of the $\vec{k} = 0$ phonons which appear near resonance[10] (up to 9 overtones have been observed for CdS[11]). By varying the temperature, a procedure that, because of the temperature dependence of the energy gap, is equivalent to varying the laser frequency, these various multiple-phonon processes can be swept through resonance, as in Ref. 10.

A peak corresponding to two LO phonons at $\vec{k} = 0$ (Γ point) has been observed to emerge at the top of the two-phonon spectrum under excitation very close to resonance in GaP.[11,12] We have studied in detail the resonance of this feature observed in the Γ_1 spectrum and shown to be similar to that of the one-LO-phonon line in a forbidden-polarization configuration. We thus conclude that the two-LO-phonon ($\vec{k} = 0$) line is due to the modulation of the elec-

tronic states through the Fröhlich interaction. This process, forbidden for one phonon if spatial dispersion is neglected, becomes allowed for two LO phonons. We have also observed in the Γ_{15} spectrum a similar resonance which corresponds to a TO-plus-LO phonon pair at Γ. This resonance, one order of magnitude weaker than that of the two LO phonons, must be attributed to a "forbidden"-deformation-potential (TO)–Fröhlich-interaction (LO) process, which becomes allowed because the k_1 of the average intervening phonon is now much larger than that of the radiation.

II. THEORY

The theory of first- and second-order Raman scattering in solids has been discussed by Ganguly and Birman.[13] We shall simplify this theory by neglecting exciton interaction, an approximation which usually holds for group-IV and -III-V semiconductors (the exciton interaction may, however, increase the strength of the Raman resonances without greatly altering their shape[14]). The first-order scattering probability is obtained in third-order time-dependent perturbation theory with the incident photon, the scattered photon, and the phonon as the perturbations. The basic diagram of this process is shown in Fig. 1, where the interaction vertices must be permuted so as to obtain five other similar terms (only Stokes processes are considered). Because of crystal-momentum conservation only phonons with $\vec{k} \simeq 0$ are excited in the first-order process, while in the second-order process $\vec{k}_1 \simeq -\vec{k}_2$. The contributions to the Raman tensor in the first-order process and in the second-order processes of type (a) have two energy denominators (notice that the structure of these processes is the same except that the electron–one-phonon interaction vertex is replaced, in the second-order processes, by an electron–two-phonon vertex). These processes fall into two categories, depending on whether the two virtual electronic excitations involved have the same (two-band terms) or different energies (three-band terms). Since the phonon energy is usually small, the two-band terms have two nearly equal energy denominators and thus resonate more strongly than the three-band contributions. The processes of type (b) have three energy denominators and therefore, when all electronic excitation energies are the same, they resonate more strongly than those of type (a). The processes of type (c) are like two consecutive first-order processes except that the photon connecting them can be virtual. Four energy denominators appear and thus stronger resonances than in all other cases are possible. These processes involve, however, six interaction vertices and thus are expected to be weaker than processes (a) and (b), which involve only three and four, respectively. The ratio of a process of type (c) to a process of type (b), involving only one electronic excitation of energy ω_0, has the form

$$\frac{I_c}{I_b} \simeq \frac{e^4}{\hbar^2 m^4} \frac{P^4}{\omega_q^4 (\omega - \omega_0)^2 V_0^2} , \tag{1}$$

where ω_q is the photon frequency which corresponds to the momentum of each of the excited phonons, P the matrix element of linear momentum, and V_0 the volume of the unit cell. Because of density-of-states considerations $\vec{q}$ is near the edge of the Brillouin zone and thus ω_q is very large. For typical values of P (0.4 a.u.) and V_0 one obtains

$$I_c/I_b \simeq 2\times 10^{-9} (\omega - \omega_0)^{-2} \quad (\text{with } \omega \text{ in eV}) . \tag{2}$$

Thus, the processes of type (c) are negligible with respect to those of type (b).

The theory just described can be considerably simplified if the phonon energies Ω can be neglected in the resonant denominators of the expressions for the Raman tensor.[15–17] This "quasistatic" approximation is justified whenever the following condition holds:

$$\Omega \ll |\omega - \omega_0 + i\Gamma| , \tag{3}$$

where ω_0 is a relevant energy gap for electronic excitations and Γ is the width of the corresponding

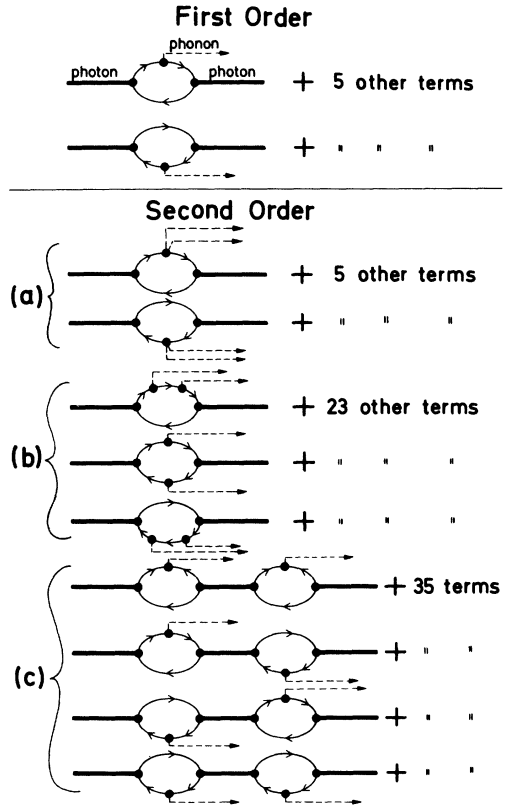

FIG. 1. Diagrams of processes contributing to first- and second-order Raman scattering.

electronic states. Under these conditions the frequency-dependent electric susceptibility of the crystal *deformed by the presence of one phonon* can be calculated using standard dielectric constant theory.[16] We can thus write, to first order in the phonon displacement ξ,

$$\chi_{ij}(\omega)=\chi_{ij}^{(0)}(\omega)+\frac{d\chi_{ij}(\omega)}{d\xi}\,\xi\,. \tag{4}$$

The phonon displacement ξ has two components of temporal dependence $e^{+i\Omega t}$ and $e^{-i\Omega t}$, corresponding to the creation and the annihilation of a phonon, respectively. Thus, upon application of an electromagnetic wave of frequency ω, one finds, according to Eq. (4), a polarization of frequency $\omega-\Omega$ (Stokes process) and $\omega+\Omega$ (anti-Stokes process): This polarization generates the scattered radiation. Crystal-momentum conservation allows only phonons with $\vec{k}\simeq 0$ to contribute to the first-order scattering process.

We shall concentrate on the Stokes process. The radiation emitted per unit time by the oscillating dipole (polarization) is, per unit area of irradiated material

$$I_R=\frac{\omega^4}{3c^3}\left|\hat{n}_k^{(i)}\frac{d\chi_{kj}(\omega)}{d\xi}\hat{n}_j^{(s)}\right|^2\langle\xi^2\rangle LE^2\,, \tag{5}$$

where L is the depth of the radiating region of the material (approximately the inverse of the absorption coefficient for strongly absorbing samples), E the magnitude of the applied field, and $\hat{n}^{(i)}$ and $\hat{n}^{(s)}$ the unit vectors along the polarization directions of the incident and scattered fields. Thus, $d\chi_{ij}(\omega)/d\xi$ is, to within a numerical constant, the Raman tensor.[18] If we take for ξ the displacement of a certain atom l of the unit cell from the equilibrium position, $\langle\xi_l^2\rangle$ is given by[19]

$$\langle\xi_l^2\rangle=\frac{\hbar}{2M_lN\Omega}\,|\vec{e}_l|^2(1+n_B)\,, \tag{6}$$

where $\vec{e}_l$ is the polarization vector of the scattering phonon at atom l, N the number of unit cells, M_l the mass of atom l, and n_B is the Bose-Einstein factor. For a germanium-type semiconductor, with two equivalent atoms per unit cell, $|\vec{e}_l|^2=\frac{1}{2}$ and the index l can be dropped in Eq. (6). In this work we discuss results for GaP, which has two atoms with different masses in the unit cell. In order to simplify our treatment we assume, however, that these masses are the same. The error introduced in this manner will be a factor of the order of 2. We believe, however, that this error is largely compensated by using in Eq. (6) twice the reduced mass for the optical phonons and the mass of Ga for the TA branches. First-order scattering is produced by phonons of $\Gamma_{25'}$ symmetry in Ge and Γ_{15} in zinc blende.

According to Eq. (5) the scattered radiation arises from the modulation in $|\chi_{ij}|$, Eq. (4), produced by the phonon displacement in a way similar to that of the external perturbations of modulation spectroscopy.[20] Two types of contributions to $d\chi_{ij}(\omega)/d\xi$ appear in the microscopic theory: those associated with a phonon-induced shift in the electronic energies and those related to phonon-induced changes in the dipole matrix elements. Energy-shift contributions correspond to the two-band processes of the general theory. Matrix-element contributions result from phonon-induced mixing of wave functions and thus correspond to the three-band processes.

In this paper, we occupy ourselves with resonances in the Raman scattering near the $E_0-E_0+\Delta_0$ gaps of GaP, which occur at the center of the Brillouin zone between the Γ_{15} spin-orbit-split ($\Gamma_8-\Gamma_7$) valence states and the Γ_1 conduction state. The phonon of Γ_{15} symmetry does not shift the energy of the Γ_1 state, and other states of Γ_{15} symmetry are sufficiently far to make contributions of Γ_1 to matrix-element changes negligible. Thus, the first-order Raman tensor arises mainly from phonon-induced perturbations of the Γ_{15} valence bands: The phonon splits the Γ_8 doublet (energy-shift contribution) while it mixes its $(\frac{3}{2},\frac{1}{2})$ component with the spin-orbit-split $(\frac{1}{2},\frac{1}{2})$ component of Γ_7. Under the assumption of a phonon-independent spin-orbit interaction the matrix elements for these two processes are not independent and only one electron-phonon coupling constant appears.[14,17] We represent this coupling constant or deformation potential by the splitting of the Γ_8 bands $\delta^{(1)}\omega_0$ produced by a phonon displacement $\xi=1$. The contribution of the $E_0-E_0+\Delta_0$ gaps to the first-order Raman tensor can thus be written (for $i\neq j$)[14,17]

$$\mathcal{P}_{ij}^{(1)}=\frac{d\chi_{ij}}{d\xi}=\frac{C_0''\delta^{(1)}\omega_0}{32\pi\omega_0}\left\{-g(x_0)+\left(4\frac{\omega_0}{\Delta_0}\right)\left[f(x_0)-\left(\frac{\omega_0}{\omega_{0s}}\right)^{3/2}f(x_{0s})\right]\right\}, \tag{7}$$

where ω_0 is the frequency of the E_0 gap, Δ_0 the spin-orbit splitting, $x_0=\omega/\omega_0$, $x_{0s}=\omega/(\omega_0+\Delta_0)$, and C_0'' is a constant related to parameters of the material and with values of the order of 1 in atomic units.[14] The functions $f(x)$ and $g(x)$ are defined by

$$\begin{aligned} g(x)&=x^{-2}\left[2-(1+x)^{-1/2}-(1-x)^{-1/2}\right],\\ f(x)&=x^{-2}\left[2-(1+x)^{1/2}-(1-x)^{1/2}\right]. \end{aligned} \tag{8}$$

It is sometimes necessary to add to Eq. (7) a real constant, to take into account all other scattering mechanisms under the assumption that they are nearly nondispersive around E_0 and $E_0+\Delta_0$.

The second-order scattering can be also treated in the quasistatic approximation, although in this case we must use in Eq. (3) $\Omega_1+\Omega_2$ instead of Ω. The quasistatic condition may therefore be more

difficult to fulfill. The second-order Raman tensor is then related to the second derivative of χ_{ij} with respect to the phonon displacements. Two different types of processes arise: those involving first derivatives of χ_{ij} with respect to electronic energies (or matrix elements) multiplied by the energy shifts (matrix-element shifts) *bilinear* in phonon displacements [i.e., processes of type (a) in Fig. 1], and those produced by second derivatives of χ_{ij} with respect to energies multiplied by energy shifts *linear* in phonon displacements [processes of type (b) in Fig. 1]. We shall consider here mainly the first type of processes since, as we shall see, they seem to dominate in our experimental work after a renormalization to take into account processes of type (b).

In a zinc-blende-type material, the second-order Raman tensor will have the three irreducible components Γ_1, Γ_{15}, and Γ_{12}, (Γ_1, $\Gamma_{25'}$, and Γ_{12} in germanium). For the E_0 and $E_0+\Delta_0$ resonances the Γ_{15} and Γ_{12} components can only act on the Γ_{15} valence bands in a manner similar to that of the Γ_{15} first-order component. The Γ_1 component can act on both Γ_1 and Γ_{15} electronic states. We would therefore expect, in the latter case, strongly dispersive energy-shift components both at E_0 and at $E_0+\Delta_0$, in contrast to the Γ_{15} and Γ_{12} cases, for which the strongly dispersive component should only occur at E_0. The Γ_{15} component of the second-order Raman tensor $\mathcal{P}_{ij}^{(2,15)}$ is then given by Eq. (7) with $\delta^{(1)}\omega_0$ replaced by $\delta_{15}^{(2)}\omega_0$, the energy splitting of Γ_8 produced by a symmetrized combination of two phonons of opposite $\vec{q}$ and unit displacements ξ. The scattering intensity for each pair of phonons is then given by

$$\frac{\omega^4}{3c^3}\left|\mathcal{P}_{ij}^{(2,15)}\right|^2\langle\xi_1^2\rangle\langle\xi_2^2\rangle LE^2 . \tag{9}$$

If we assume $\mathcal{P}_{ij}^{(2,15)}$ independent of $\vec{k}$ (or if we use the appropriate average), the spectral distribution of the intensity scattered by all possible pairs of phonons from two given branches is obtained by multiplying Eq. (9) by the appropriate combined density of states. In order to obtain the total scattered intensity we must multiply Eq. (9) by $N/2$, the total number of phonon pairs, and a degeneracy factor η, which can be larger than 1 if transverse phonons contribute; we then obtain

$$\frac{\omega^4}{3c^3}\langle\left|\mathcal{P}_{ij}^{(2,15)}\right|^2\rangle\langle\xi_1^2\rangle\langle\xi_2^2\rangle LE^2N(\eta/2) . \tag{10}$$

We shall usually assume that $\mathcal{P}_{ij}^{(2,15)}$ is independent of the $\vec{k}_1\simeq-\vec{k}_2$ of the individual phonons, an assumption justified by the fact that the obtained spectra reproduce rather well the features of the combined density of states. Under these conditions

$$\langle\left|\mathcal{P}_{ij}^{(2,15)}\right|^2\rangle=\left|\mathcal{P}_{ij}^{(2,15)}\right|^2 .$$

The ratio of the first- to second-order scattered intensities is given by

$$\frac{I^{(2,15)}}{I^{(1)}}=\left(\frac{\delta_{15}^{(2)}\omega_0}{\delta^{(1)}\omega_0}\right)^2\frac{\langle\xi_1^2\rangle\langle\xi_2^2\rangle N}{\langle\xi_0^2\rangle}(\eta/2) . \tag{11}$$

Thus, by calculating $\langle\xi_1^2\rangle$ with Eq. (6) we can obtain from the observed ratio of scattered intensities the ratio of the second- to the first-order coupling constants.

We consider next the Γ_{12} component of the Raman tensor. If we designate by X, Y, Z the phonons polarized along the crystal axes, the two-phonon states of Γ_{12} symmetry are

$$\begin{aligned}|12\rangle_1&=XX+YY-2ZZ ,\\ |12\rangle_2&=\sqrt{3}\,(XX-YY) .\end{aligned} \tag{12}$$

The Γ_{12} component of the Raman tensor is characterized by its $\mathcal{P}_{11}^{(2)}$ component, which is given by an expression similar to Eq. (7) with $\delta^{(1)}\omega_0$ replaced by $\delta_{12}^{(2)}\omega_0$ [the energy splitting of the Γ_8 valence state produced by the two-phonon states of Eq. (12) with phonon displacements of unit amplitude]. Using Loudon's notation for the Raman tensor,[18]

$$\begin{aligned}d^{(1)}&=\mathcal{P}_{12}^{(1)}\langle\xi_0^2\rangle^{1/2} ,\\ b^{(2)}&=\mathcal{P}_{11}^{(2,12)}\langle\xi_1^2\rangle^{1/2}\langle\xi_2^2\rangle^{1/2}N(\eta/2) .\end{aligned} \tag{13}$$

We can express the ratio of the strengths of the Γ_{12} component of the second-order spectrum to that of the first-order spectrum as

$$\left(\frac{b^{(2)}}{d^{(1)}}\right)^2=\left(\frac{\delta_{12}^{(2)}\omega_0}{\delta^{(1)}\omega_0}\right)^2\frac{\langle\xi_1^2\rangle\langle\xi_2^2\rangle N}{\langle\xi_0^2\rangle}(\eta/2) . \tag{14}$$

Thus, within our approximations the shape of the resonance in the Γ_{12} two-phonon spectrum should also be the same as that of the Γ_{15} one-phonon scattering.

We consider now the Γ_1 component of the two-phonon spectrum for which, as we have already mentioned, a different situation arises. We assume, for simplicity, that the two-phonon combination of Γ_1 symmetry,

$$\tfrac{1}{3}(XX+YY+ZZ) , \tag{15}$$

acts only on the Γ_1 conduction state; we shall see later that the effect of this mode on the Γ_{15} states is usually negligible. The ratio of the Γ_1 scattering strength to that of the first-order spectrum per phonon branch is given by[14] (in Loudon's notation)

$$\left(\frac{a^{(2)}}{d^{(1)}}\right)^2=\left(\frac{4\delta_1^{(2)}\omega_0}{\delta^{(1)}\omega_0}\right)^2\frac{\langle\xi_1^2\rangle\langle\xi_2^2\rangle N}{\langle\xi_0^2\rangle}\times\left|\frac{g(x_0)+3f(x_0)+\frac{1}{2}[g(x_{0s})+3f(x_{0s})]-C}{-g(x_0)+(4\omega_0/\Delta_0)[f(x_0)-(\omega_0/\omega_{0s})^{3/2}f(x_{0s})]}\right|^2\frac{\eta}{2} , \tag{16}$$

where $\delta_1^{(2)}\omega_0$ is the energy shift of the Γ_1 conduction

state produced by Eq. (15) with phonons of unit amplitude. We have included the real constant C in the numerator of Eq. (16) in order to take into account a possible dispersionless background. The consideration of this background is particularly important in connection with Γ_1 scattering. The function $g(x_0)+3f(x_0)$ tends to zero for $x_0 \to 0$, thus revealing any possible background far from the gap. A similar effect does not take place for Γ_{15} and Γ_{12} scattering.

In the limit $\Delta_0 \ll \omega_0 - \omega \ll \omega_0$, Eq. (16) reduces to

$$\left(\frac{a^{(2)}}{d^{(1)}}\right)^2 = \left(\frac{2\delta_1^{(2)}\omega_0}{\delta^{(1)}\omega_0}\right)^2 (\eta/2) \ . \tag{17}$$

We proceed now to the microscopic calculation of $\delta_1^{(2)}$, $\delta_{15}^{(2)}$, and $\delta_{12}^{(2)}$. For the sake of simplicity we shall assume that the two atoms per unit cell have the same mass (group-IV materials). In the case of the III-V compounds this approximation would be satisfactory for GaAs, although it should lead to some error for GaP. The microscopic theory of $\delta^{(1)}\omega_0$ has been discussed by Cerdeira and Cardona.[21] These authors find

$$\delta^{(1)}\omega_0 = (2/a_0)\, d_0 \ , \tag{18}$$

with a_0 equal to the lattice constant and $d_0 = 33$ eV for germanium.

The electron–two-phonon interaction Hamiltonian is[22,23]

$$H_{ep}^{(2)} = \frac{1}{2}\sum_{RR'} \vec{\xi}_1(\vec{R}) \cdot (\vec{\nabla}_{\vec{R}}\, \vec{\nabla}_{\vec{R}'}\, V) \cdot \vec{\xi}_2(\vec{R}') \ , \tag{19}$$

where V is the crystal potential, $\vec{R}$ the position vector of an arbitrary atom, and $\vec{\xi}(\vec{R})$ the corresponding phonon displacement. In the rigid-ion approximation[23] only diagonal terms in R and R' survive and Eq. (19) becomes

$$H_{ep}^{(2)} = \frac{1}{2}\sum_{R} \vec{\xi}_1(\vec{R}) \cdot (\vec{\nabla}_{\vec{R}}\, \vec{\nabla}_{\vec{R}}\, V) \cdot \vec{\xi}_2(\vec{R}) \ . \tag{20}$$

The contributions of each of the two basis atoms to Eq. (20) have the same sign if we deal with two phonons of the same kind (acoustical-acoustical, optical-optical). If we deal with combinations of one acoustical and one optical phonon, both contributions have opposite sign and they cancel: Thus, only weak acoustical-optical combination scattering is expected, a fact which is confirmed by experiment.[5,7] We also notice that the two-phonon interaction for a pair of optical phonons is equal to that for a pair of acoustical phonons,[23] a fact which agrees well with second-order Raman scattering in Si,[7] but not so well for Ge[5] and GaP.[8] The expectation value of Eq. (20) for an electronic state of periodic Bloch function χ is

$$\delta_{\ell_1,\ell_2}^{(2)}\omega_0 = \langle \chi | H_{ep}^{(2)} | \chi \rangle = \int_{V_0} \chi^* \chi (\vec{\xi}_1 \cdot \vec{\nabla})(\vec{\xi}_2 \cdot \vec{\nabla} V)\, d\tau \ , \tag{21}$$

where $\vec{\xi}$ gives the amplitude and the direction of the phonon-induced displacement of an atom, and V_0 is the volume of the unit cell. Replacing the symmetrized combination of Eq. (15) into Eq. (21) we find

$$\delta_1^{(2)}\omega_0 = \tfrac{1}{3}\int_{V_0} \chi^* \chi \nabla^2 V\, d\tau = (4/3a_0^2)\, D_1 \ , \tag{22}$$

where D_1 is the constant defined in Ref. 23. The degeneracy factor η of Eq. (16) equals 1 for two-LO and 2 for two-TO scattering.

Because of the strong divergence in the crystal potential near the atomic core, the main contribution to Eq. (22) is produced in this region. If we approximate V by the sum of the Coulomb potentials $-Ze^2/r$ at the atomic sites we find from Eq. (22)

$$D_1 = 2\pi a_0^2 Ze^2 |\chi(0)|^2 \ . \tag{23}$$

Thus, within the range of validity of this approximation the "deformation potential" D_1 vanishes unless the wave function χ has an s-like component. We therefore conclude that D_1 vanishes for the Γ_{15} valence states while it has a finite value for the Γ_1 conduction band. The deformation potential D_1 can be estimated from Eq. (23) by replacing $\chi(0)$ with its value for the isolated atom. Using the tables of Herman and Skillman[24] we find for germanium $D_1 = 3\times10^6$ eV, an extremely large value. Using orthogonalized-plane-wave (OPW) wave functions and the complete crystal potential, Lin-Chung and Ngai[23] obtained $D_1 = 3\times10^5$ eV.

At this point it is interesting to reflect that if one moves adiabatically the core of an isolated atom the energies of its various levels do not change: The wave functions deform so as to adapt themselves to the new shifted potential without energy change. Thus, the effect of the perturbation represented by $\nabla^2 V$ and taken to first order must be compensated by terms of the form $\vec{\nabla} V$ taken to second order through all possible intermediate states. In the solid, the wave functions are Bloch waves and they cannot completely follow the core deformations (if they did D_1 would be zero). This argument, which seems to have been overlooked in Ref. 23, is similar to that presented by Herring.[25] In order to avoid the sum of second-order terms over all possible intermediate states we make the reasonable assumption that in the OPW formulation the core contributions to the wave function deform with the potential while the plane-wave parts do not. Using for Γ_1 the plane waves given in Ref. 14 we find $D_1 = 1.8\times10^4$ eV.

As discussed earlier, the contribution to the second-order Raman scattering by first- and second-order terms in the electron-phonon interaction must be treated separately [(b) and (a) diagrams of Fig. 1, respectively]. In a two-band model of resonant scattering, however, one can sum all possible first-order type-(b) terms which connect the two bands with other bands far away from the resonant

gap. This sum has a behavior similar to that of the type-(a) terms of Fig. 1. We can therefore eliminate the first-order interaction and calculate only terms of the type (a) with an electron–two-phonon interaction vertex renormalized so as to include the electron–one-phonon interaction via intermediate states. This renormalization is analogous to the cancellation of D_1 just described: The first-order electron–two-phonon terms are partly canceled by second-order terms from the electron–one-phonon interaction. Thus, the $\delta^{(2)}\omega_0$ which appear in Eqs. (11), (14), and (16), and the corresponding electron–two-phonon deformation potentials D, should be renormalized as described. We should emphasize the fact that this renormalization assumes that all additional intermediate states in the terms of type (b) are far from resonance. Otherwise one would obtain terms of type (b) which resonate more strongly than those of type (a), and thus must be included explicitly when approaching the resonance. We shall see that because of the near degeneracy of the Γ, L, X, and W conduction-band points in GaP such terms seem to appear but only very near the resonance.

Ngai and Johnson[23] found for InSb, from an analysis of two-phonon-aided cyclotron resonance, $D_1 = (5.6\times10^4/\bar{p}^{1/2})$ eV, where $\bar{p}$ is a weighting factor of the order of but smaller than 1. This result should also include the renormalization just mentioned, and thus is in qualitative agreement with the result of our calculation for Ge(1.8×10^4 eV). Because of the larger atomic number of InSb we would expect [see Eq. (23)] for the D_1 of this material a value somewhat larger than that of germanium. Such value is obtained from the experiment of Ref. 23, since, as already mentioned, $\bar{p}<1$.

We shall now discuss the microscopic theory of $\delta_{15}^{(2)}\omega_0$. We define this energy as the splitting of the Γ_8 level obtained for phonons of unit displacement polarized along [111]. We find from Eq. (21)

$$\delta_{15}^{(2)}\omega_0 = 2\int_{V_0} \chi_x^* \chi_y \frac{\partial^2 V}{\partial x \partial y}\, d\tau = \frac{4}{a_0^2} D_{15} . \tag{24}$$

Equation (24) defines the deformation potential D_{15}. The degeneracy factor η equals 2 for LO-TO scattering.

Under the assumption of pure atomic p wave functions the functions χ_x and χ_y have the form $\chi_x = xR(r)$ and $\chi_y = yR(r)$. If we additionally assume a Coulomb potential, Eq. (24) can be transformed into

$$D_{15} = -\frac{a_0^2}{15}\int_{V_0} r|R(r)|^2 \frac{dV}{dr}\, d\tau . \tag{25}$$

In this case the spin-orbit splitting of the valence band is

$$\Delta_0 = \frac{\hbar^2}{4m^2c^2}\int_{V_0} r|R(r)|^2 \frac{dV}{dr}\, d\tau . \tag{26}$$

We thus find the following relationship between D_{15} and Δ_0:

$$D_{15} = -\frac{4m^2c^2a_0^2}{15\hbar^2}\Delta_0 = -5.5\times10^5\,\Delta_0 . \tag{27}$$

Equation (27) yields for Ge, with $\Delta_0 = 0.3$ eV, $D_{15} = 1.7\times10^5$ eV. We would also expect the renormalization discussed above to apply in this case, and hence this value of D_{15} should be an upper limit: The correct value should be about two orders of magnitude smaller.

Because of the isotropy built into the present model, it is not necessary to calculate explicitly D_{12}. We would simply expect $\delta_{15}^{(2)}\omega_0 = \delta_{12}^{(2)}\omega_0$.

The theory of the forbidden one-LO-phonon scattering has been discussed by a number of authors.[26–29] Forbidden scattering is much weaker for the TO phonon and is negligible in nonpolar materials such as germanium. Therefore the mechanism responsible for the violation of the selection rule must be related to a specific property of the longitudinal phonons, namely, to the electric field which accompanies them. This electric field can produce intraband scattering of electrons (Fröhlich interaction). Thus, a scattering mechanism different from the deformation potential theory discussed so far arises: the intraband scattering of electrons by phonons via Fröhlich interaction. A detailed calculation[26–29] shows that this mechanism is only effective when the direction of polarization of the incident radiation is parallel to that of the scattered radiation. The corresponding Raman tensor turns out to be proportional to the magnitude of the scattering wave vector $\vec{q}$ and vanishes for $\vec{q}=0$: The selection rule is lifted because of the finite magnitude of $\vec{q}$.[30]

Strong electric fields are often present at the surface of semiconductors. These electric fields can also produce a breakdown in selection rules and allow the forbidden LO scattering. The scattering probability is proportional to[27]

$$\left|\tfrac{1}{2}[(m_e^2 - m_h^2)/m^2]q - i\tfrac{9}{4}\mathcal{S}\right|^2 , \tag{28}$$

where $\mathcal{S}$ is the magnitude of the applied field, m_e and m_h the electron and hole masses, and $M = m_e + m_h$. Evidence of both types of LO-forbidden scattering mechanisms, $\vec{q}$ induced[30] and surface field induced,[31] has been presented in the literature. As a forbidden process, the LO-forbidden scattering is expected to resonate more sharply near E_0 than the corresponding allowed processes. Detailed calculations of the shape of this resonance have appeared, in particular, a recent one which covers the energy range below and above E_0.[29] If exciton interaction is neglected (an approximation probably valid for GaP, but not for II-VI compounds[26]) we expect the leading term in the Raman tensor of the $\vec{q}$-induced process to be proportional to the derivative

of the corresponding term in the allowed Raman tensor [$\sim(\omega-\omega_0)^{-1/2}$]. We thus conclude that the forbidden scattering intensity should have $(\omega-\omega_0)^{-3}$ as its leading term near E_0.

In our experiments we observe a strong resonance of the structure which corresponds to emission of two LO-phonons with $\vec{k}\simeq 0$. Equation (28) provides a simple scattering mechanism for this process: The "forbidden" scattering by one of the two phonons is being induced by the electric field which accompanies the other LO-phonon. One could view this process heuristically in the sense of Eq. (28): One phonon provides the $\vec{q}$, which now is $\vec{k}_1$ and not the scattering $\vec{q}$ vector, and the other provides the electric field. Thus, the two-LO (Γ) process becomes allowed (it is independent of the scattering $\vec{q}$ vector) and is expected to have a resonance shape analogous to that of the forbidden one-LO scattering. We must, however, provide a cutoff mechanism to limit the $\vec{k}_1\simeq\vec{k}_2$ of the emitted phonons to a region near $\vec{k}=0$. This mechanism is provided by the fact that as $\vec{k}_1$ increases one of the energy denominators becomes nonresonant, since the intermediate state moves away from $\vec{k}=0$. In the case of an exciton-enhanced process, the cutoff is provided by the fact that the phonon wavelength $2\pi/\vec{k}_1$ must be larger than the Bohr radius of the exciton.[11]

III. EXPERIMENT

The GaP sample was an undoped single crystal ($n\simeq 10^{15}$ cm^{-3}). It was oriented by conventional x-ray techniques to $\pm 1°$, mechanically polished, and well etched in a dilute solution of bromine in methanol. The backscattering configuration was used throughout, the scattering surface being usually $(\bar{1}10)$. For the resonance measurements the incident and scattered light was polarized in the plane of the sample with the electric field parallel to the [111] direction. The allowed symmetry composition of the measured cross section for this configuration is $\Gamma_1+\frac{4}{3}\Gamma_{15}$ ($a^2+\frac{4}{3}d^2$ in the notation of Loudon).[18] The first-order TO (Γ) phonon is allowed and occurs at 365.5 cm^{-1} in the Γ_{15} component. The first-order LO (Γ) phonon, however, is always forbidden for backscattering from a $(\bar{1}10)$ plane.

We also performed some measurements for different polarization configurations of the incident and scattered light at exciting frequencies of 4579 Å (Ar ion) and 4416 Å (He-Cd) so as to sort out at frequencies close to the resonant gap which of the observed features belong to Γ_{15}, Γ_{12}, and Γ_1. The results for 4579 Å in the two-optical-phonon region are shown in Fig. 2. The second-order Raman spectrum of this material[8] has been previously studied in detail far below the E_0 gap (5145-Å exciting frequency), and a complete decomposition of the spectrum into the irreducible components of the Raman tensor (Γ_1, Γ_{12}, Γ_{15}, for a zinc-blende-type material) has been performed. It was found, for the most part, that the Γ_{15} component does not interfere with the Γ_1 component, the corresponding structure being mutually exclusive owing to the *combination* nature of the former and the *overtone* nature of the latter. For example, in the optical region the structure *between* the strong Γ_1 scattering due to TO overtones (660–735 cm^{-1}) and that due to LO overtones (770–810 cm^{-1}) is of Γ_{15} symmetry (refer to Fig. 2), being composed of TO plus LO combination states. The symmetry mixture $\Gamma_1+\frac{4}{3}\Gamma_{15}$ was chosen because it exhibits all of the major features of the spectrum, and emphasizes the Γ_{15} component which is otherwise small compared to Γ_1. We felt that the Γ_{12} component was too small for a meaningful study of resonance effects. The tensor symmetry of the various structures does not depend on exciting frequency. This fact was established by separating the irreducible components of the Raman tensor at 4579 and 4416 Å.

At room temperature the E_0 exciton gap in GaP occurs at 2.78 eV and the corresponding $E_0+\Delta_0$ gap at 2.86 eV.[32,33] Since the exciton binding energy is rather small (0.01 eV), we shall therefore make no distinction between exciton gap and band edge. The available lasers appropriate for the study of resonance effects in the region of the E_0, $E_0+\Delta_0$ gaps of GaP are the Argon-ion and He-Cd lasers, the former providing several lines in the region 2.41 eV (5145 Å) to 2.708 eV (4579 Å), and the latter having a line at 2.808 eV (4416 Å). In order to thoroughly study the resonant region the Raman spectrum was recorded at room temperature with 5145-, 4880-, 4765-, and 4579-Å (Argon-ion) exciting light, and at several temperatures with 4416-Å (He-Cd) exciting light. By varying the temperature between 77 and 670 °K it was possible to tune the E_0 gap from 2.865 eV to 2.592 eV,[32,33] through the He-Cd laser

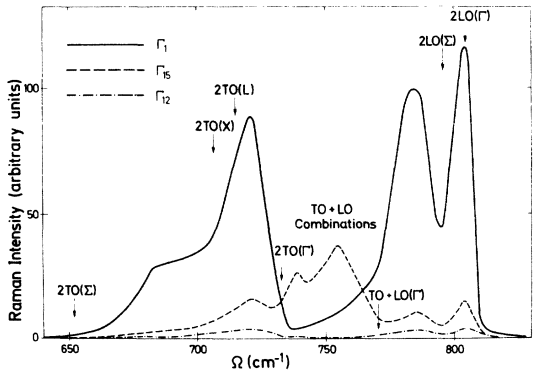

FIG. 2. Three irreducible components of the Raman tensor of GaP in the region of scattering by two optical phonons. Recorded at room temperature with 4579-Å exciting light.

line (2.808 eV). Except for some increase in the lifetime broadening as the temperature is raised, the effect of changing the temperature is equivalent to changing the photon energy of the laser by an amount equal in magnitude and of opposite sign to the corresponding change in the gap.[10] Thus it was possible to measure the Raman spectrum for a fine mesh of scattering photon energies (or their temperature-tuned equivalent) covering the region from

$$\omega_L - \omega_0 = -0.367 \text{ eV} \quad \text{to} \quad \omega_L - \omega_0 = +0.216 \text{ eV}.$$

All measurements were performed with the sample glued (GE 7031 varnish) to the copper finger of an optical Dewar designed to cover the temperature range of interest. Cooling was accomplished with dry ice, dry ice in acetone, and liquid N_2. Heating was performed with a ceramic resistor mechanically attached to the copper finger. The temperature was measured with a calibrated iron-constantan thermocouple, also mechanically clamped to the finger near the crystal. During the measurements the sample was kept in a vacuum of $\sim 10^{-5}$ torr.

A Spex triple monochromator system was employed with detection by photon counting. The Stokes spectrum was recorded as a function of scattered frequency in the 1024 channels of a multichannel analyzer and then plotted and printed to give both a graphic and a tabulated result. The spectrometer slits were chosen to yield a resolution of 6 cm^{-1}. At this resolution no significant broadening of any of the observed phonon lines is seen with increasing temperature, and thus the height of the peaks gives a measure of their strength. In order to avoid appreciable heating of the scattering portion of the sample we kept the laser power low (50–100 mW) and focused the laser light with a cylindrical lens. We checked the absence of heating by measuring the absolute wave number of the first-order lines and showing that it was independent of laser power in this range.

Two sets of measurements were performed. In the first set the resonant behavior of the TO (Γ) and the forbidden-LO (Γ) peaks was carefully measured. Particular attention was paid to the alignment and focus of the optics so as to reproduce the experimental conditions for each exciting laser line and temperature. The laser power was recorded before and after each run, and the spectrometer response was carefully calibrated by measuring the Raman scattering from a CaF_2 crystal for the same exciting lines. This material, with a gap of about 11 eV, should yield a scattering cross section proportional to ω_L^4, without any dispersion due to energy denominators. The ratios of the TO (Γ) and forbidden-LO (Γ) one-phonon lines to the corresponding CaF_2 intensity are then automatically corrected for spectrometer response, and the ω_L^4 frequency factor in the scattering cross section is eliminated.

In the second set of measurements we were concerned more with the second-order than with the first-order spectrum. Once the resonant behavior of the first-order TO (Γ) peak is well known it is not necessary to measure as carefully the absolute resonant behavior of the second-order spectrum. It suffices to measure its change in intensity with respect to the first-order TO (Γ) peak. Therefore, for these measurements the scattered intensity was always divided by the TO (Γ) peak intensity recorded during the same run. The resulting ratio is automatically corrected for spectrometer response, incident laser power, the ω_L^4 factor in the scattering cross section, and even any changes in the optical alignment which might occur in going from one exciting laser line or temperature to the next. We found that this procedure yields accurate and reproducible results.

For both the first- and second-order measurements the data taken at different temperatures were corrected for statistical factors by multiplying the experimental cross section by the ratio of the appropriate Bose factors at 300 °K to the factors at the temperature of the measurement. Thus, all data presented here are referred to room temperature. In passing through the direct gap the absorption changes rapidly, and it is necessary to correct the data for the change in penetration depth of the light by multiplying the cross section by the sum of the incident and scattered absorption constants.[34] Using the data of Refs. 32 and 33 we have corrected our measurements for absorption as a function of the scattered frequency taking account of the shift and broadening of the gap and exciton peaks as the temperature is increased. When performing relative measurements with respect to the first-order spectrum, the absorption correction is mostly eliminated, but not completely because of slight differences in the scattered frequencies. We performed the absorption correction also in these cases by using the data of Refs. 32 and 33.

IV. RESULTS

Figure 3 shows the resonant behavior of the allowed first-order TO (Γ) mode of Γ_{15} symmetry in the region of the E_0 and $E_0 + \Delta_0$ gaps. These data give the results of the careful first-order measurements previously described in Sec. III. The present measurements (crosses) and the measurements of Scott *et al.*[12] (squares) are both plotted. The agreement between these two sets of data is good below the E_0 gap; the region above the E_0 gap has not been previously explored. The solid and dashed lines are computer plots of the theoretical expressions for the square of the first-order Raman tensor developed in Sec. II, Eqs. (7) and (8). They are fitted to the experimental point at $\omega_L - \omega_0$

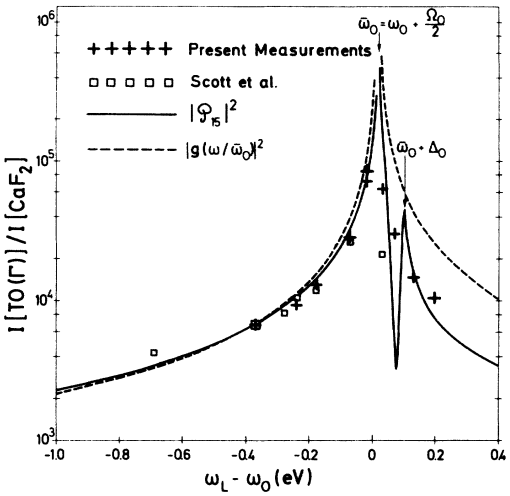

FIG. 3. Raman cross section as a function of incident photon energy for the first-order allowed TO (Γ) phonon. The room-temperature E_0 gap is the zero of the horizontal scale. The data of Ref. 12 (squares) have been adjusted to correspond to our data (crosses) at $\omega_L-\omega_0 = -0.367$ eV. The functions $\mathcal{P}_{15}$ [Eq. (7)] and g [Eq. (8)] have also been adjusted to fit the same data points with a multiplicative constant. As explained in the text, the data have been corrected for absorption, spectrometer response, statistical factors, etc.

$= -0.367$ eV (5145-Å exciting line) by adjusting a multiplicative constant (vertical shift in the log plot of this figure). We replace the singular gap ω_0 in Eqs. (7) and (8) by $\bar{\omega}_0=\omega_0+\Omega_0/2$, where Ω_0 is the TO (Γ) phonon frequency, since we do not expect to resolve the separate resonances due to the incident and scattered photon energies. In this manner, the theoretical curves are forced to peak at $\bar{\omega}_0$. The dashed line in Fig. 3 is $|g(x_0)|^2$ of Eq. (8). It fits the experimental points very well below the E_0 gap, where the contribution of the f function to the Raman tensor in Eq. (7) is small, but is too large above the gap. Effects of the spin-orbit split $E_0+\Delta_0$ gap are not included in $|g(x_0)|^2$. The solid line, $|\mathcal{P}_{15}|^2$, is a plot of the square of the function in brackets in Eq. (7). This function is the contribution to the Raman tensor of the effect of a deformation of Γ_{15} symmetry on the valence bands; it includes the effect of the spin-orbit-split gap. As previously discussed, the main resonance occurs at the E_0 gap [g function, singular behavior $\propto(\omega-\bar{\omega}_0)^{-1/2}$] with a secondary weaker peak [f function, singular behavior $\propto(\omega-\bar{\omega}_0-\Delta_0)^{1/2}$] at $E_0+\Delta_0$. Between these two peaks $|\mathcal{P}_{15}|^2$ shows a minimum which is not resolved in the experiment (we should emphasize that the measurements in this region were taken at high temperatures). This function provides an excellent fit to the data below the gap and also above the gap if we slightly broaden the minimum and subsequent maximum at $E_0+\Delta_0$. Low-temperature experiments using a pulsed-nitrogen-dye-laser system are presently being performed in our laboratory in order to try to resolve the minimum in the calculated curve of Fig. 3.

In Fig. 4, we display the second-order Raman spectrum of GaP between 100 and 860 cm^{-1} measured for four different values of $\omega_L-\omega_0$ (exciting light of wavelength 5145 Å, at room temperature, and 4416 Å at 78, 356, and 625 °K). These spectra have been normalized to the intensity of the first-order TO (Γ) peak, as explained in Sec. III. Therefore, in this figure the TO (Γ) peak always

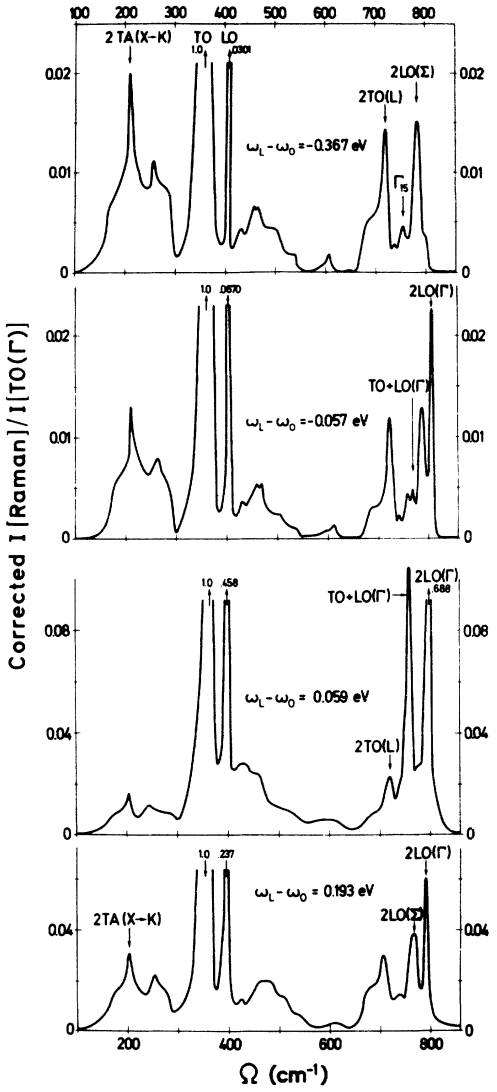

FIG. 4. Raman spectrum of GaP between 100 and 860 cm^{-1} normalized to the first-order TO (Γ) intensity. The four spectra were recorded (from top to bottom) with 5145-Å exciting light at 300 °K and with 4416-Å exciting light at 78, 356, and 625 °K, respectively. The spectra have been corrected for absorption and statistical factors. (They are referred to 300 °K.)

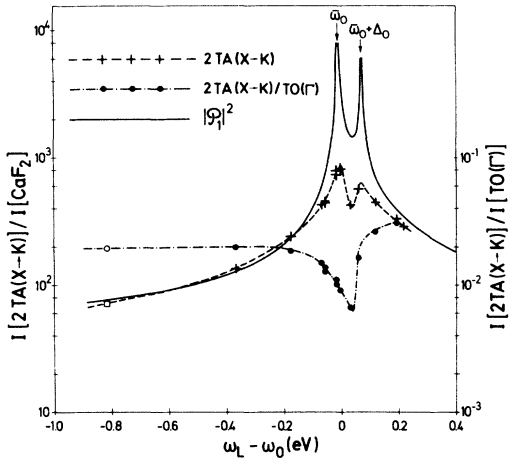

FIG. 5. Resonance of the two-TA ($X \rightarrow K$) Raman peak in the region of the E_0, $E_0+\Delta_0$ gaps of GaP as a function of incident laser frequency. The E_0 gap occurs at the zero of the horizontal scale. The dots are the ratios of the peak intensity to the height of TO (Γ). The crosses display the absolute resonant behavior of two-TA ($X \rightarrow K$); they are the results of multiplying this ratio by the separate TO (Γ) intensities obtained from Fig. 3. The data have been corrected for absorption, statistical factors (referred to 300 °K), etc. The constant C in the function $|\Phi_1|^2$ [numerator of Eq. (16)] has been chosen to be 2.5 so as to give the best fit to the experimental points. The circle and square are points from Ref. 39.

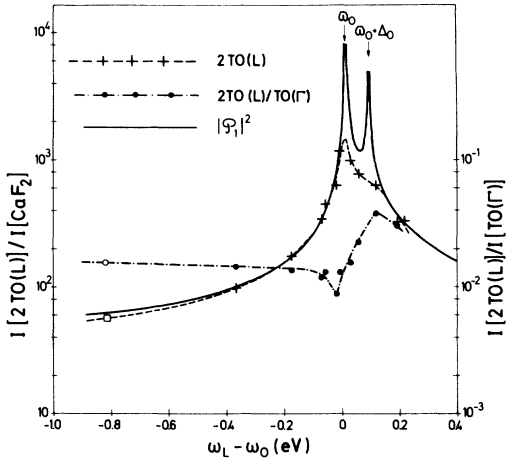

FIG. 6. Resonant behavior of the two-TO (L) peak in the region of the E_0, $E_0+\Delta_0$ gaps. See caption of Fig. 5 for details (C has also been taken to be 2.5).

has a maximum height of 1. The spectra have been corrected for absorption and statistical factors in the manner described in Sec. III. It is evident that two effects are taking place: The over-all intensity of the spectrum is changing with exciting frequency in a manner similar but not exactly the same as the TO (Γ) peak. At the same time two additional sharp peaks appear when the laser frequency (or its temperature-shifted equivalent) is near the gap (He-Cd laser, 356 °K) and disappear again above the gap (same laser, 625 °K). Thus, these two peaks resonate much more strongly than TO (Γ). The strongest of these peaks occurs at a wave number which corresponds to the excitation of two LO phonons at Γ (overtone), while the other, somewhat weaker one seems due to the simultaneous excitation of one TO and one LO phonon near Γ [TO-plus-LO (Γ) combination].

We shall deal first with the over-all spectrum, which can be divided into its irreducible components of Γ_1 and Γ_{15} symmetry (neglecting, as we have already mentioned, the small Γ_{12} component). As representative of the Γ_1 spectrum we have plotted in Figs. 5–7 the resonant behavior of the strongest overtone peaks [two TA ($X \rightarrow K$), two TO (L), and two LO (Σ), respectively, see Ref. 8]. In these figures the points with the dashed-dotted line running through are the directly measured ratios of the height of the peak under consideration to that of the TO (Γ) peak. The crosses with the dashed line running through give the absolute resonant behavior of the mode. They are the result of multiplying the ratios of the dashed-dotted curves by the TO (Γ) intensity of Fig. 3. The solid doubly peaked curves represent the theoretical expression found in Sec. II [numerator of Eq. (16)] for the contribution to the second-order Raman scattering of Γ_1 symmetry, the function

$$\Phi_1 = g(x_0) + 3f(x_0) + \tfrac{1}{2}[g(x_{0s}) + 3f(x_{0s})] - C$$

describing the effect of a hydrostatic deformation on either the Γ_1 conduction or the Γ_{15} valence states. In this equation $x_0 = \omega/\overline{\omega}_0$, with $\overline{\omega}_0$ taken to be the frequency at which the main peak in the experimen-

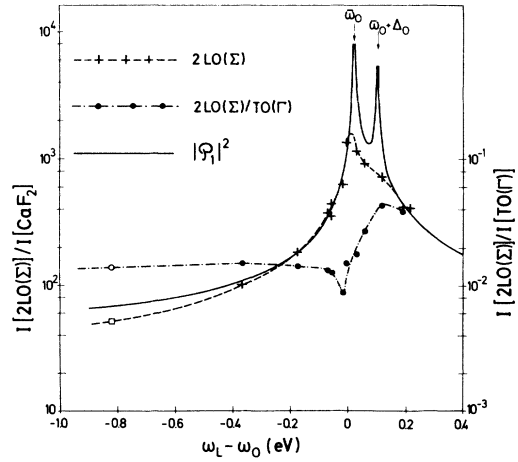

FIG. 7. Resonant behavior of the two-LO (Σ) mode in the region of the E_0, $E_0+\Delta_0$ gaps. See caption of Fig. 5 for details (C has also been taken to be 2.5).

tal Raman resonance occurs. $\bar{\omega}_0$ agrees with the theoretical value $\omega_0+(\Omega_1+\Omega_2)/2$ in Fig. 5, but is 0.025 eV lower in Figs. 6 and 7. Resonant frequencies similarly lower than the theoretical ones also appear in other Raman work.[35] The real constant C has been subtracted to take into account a possible background. [Note that $3f(x_0)+g(x_0)$ tends to zero for $x_0 \to 0$. Thus a background is bound to become important at sufficiently low frequencies.] $|\mathcal{P}_1|^2$ shows two resonances, at the E_0 and $E_0+\Delta_0$ gaps, with the E_0 resonance twice as strong because of the double degeneracy of this valence band. The best fit to our data was obtained by varying the background constant C. The same value of $C=2.5$ was used for $|\mathcal{P}_1|^2$ in all three figures.

The two-TA($X \to K$) mode, Fig. 5, clearly shows a double resonance with two peaks occurring at E_0 and $E_0+\Delta_0$. In this respect the agreement with theory is quite satisfactory although the theoretical curve predicts a stronger resonance (see Sec. V).

The resonant behavior of the two-TO (L) and two-LO (Σ) modes (Figs. 6 and 7, respectively) is very similar. Good agreement with the theoretical curve is obtained again, especially if one takes into account lifetime broadening in the experiment (the data around $E_0+\Delta_0$ were obtained at high temperatures). The spin-orbit-split resonance, however, is somewhat less well defined than in the two-TA ($X \to K$) case. This may be the result of the breakdown of the quasistatic model, which assumes phonon frequencies much less than the spin-orbit splitting. The energy of these modes is about 0.1 eV, whereas the spin-orbit splitting is 0.082 eV. In contrast, the two-TA($X \to K$) energy is approximately 0.025 eV.

In Fig. 8 we display the resonant behavior of the major peak occuring at 755 cm^{-1} in the Γ_{15} component of the optical spectrum. We have chosen to study the resonant behavior of this peak in detail as a typical example of the Γ_{15} Raman component. Again the points with dashed-dotted line are the ratios of the peak intensity to TO (Γ), and the crosses with dashed line are those ratios multiplied by the separate TO (Γ) measurements of Fig. 3. The theoretical curve (solid line), $|\mathcal{P}_{15}|^2$, is the solid line in Fig. 3 [Eq. (7)], fitted to the experimental point at $\omega_L-\omega_0=-0.367$ eV by adjusting a multiplicative constant (vertical shift on the log plot of Fig. 8) and with the singularity at the appropriate $\bar{\omega}_0$. From the good fit of the data to this curve and the near constancy of the ratios to TO (Γ), it is clear that this peak in the Γ_{15} component of the second-order spectrum is resonating just like the first-order allowed TO (Γ) phonon below the gap, in agreement with Eq. (7). If some background is present, other than the explicit E_0, $E_0+\Delta_0$ contributions of Eq. (7), it must be the same for both the TO (Γ) and the two-phonon combination processes. From the good fit of the theoretical curves in Figs. 3 and 8 we conclude that any possible background term is very small.

Unfortunately, we were not able to obtain any points for Fig. 8 above the E_0 gap because the corresponding structure becomes obscured by the strongly resonating TO-plus-LO (Γ) peak (see Fig. 4). It is evident from our data that the behavior of other structure in the Γ_{15} component of the scattering [with the exception of the TO-plus-LO (Γ) peak] is similar and can be equally well explained by Eq. (7) as a modulation of the valence bands by a deformation of Γ_{15} symmetry.

The forbidden first-order LO (Γ) peak, the TO-plus-LO (Γ) combination occurring in the Γ_{15} component, and the two-LO (Γ) overtone occurring in Γ_1 all resonate much more strongly than the allowed TO (Γ) phonon. This becomes evident in Fig. 4 where the ratio of these peaks to TO (Γ) changes drastically as the gap is traversed. Figures 9–11 display the resonant behavior of the forbidden LO (Γ), TO-plus-LO (Γ), and two-LO (Γ) peaks, respectively. The crosses are our experimental points; again they are obtained by multiplying the ratio of the mode intensity to TO (Γ) by the separate first-order measurements of TO (Γ) (Fig. 3) and are corrected for temperature and absorption as discussed in Sec. III. The solid line is a theoretical calculation of the Raman cross section for the forbidden LO scattering performed by Zeyher *et al.*[29] (see Sec. V).

In Fig. 9 we see that the agreement of the calculation with our measurements for the forbidden first-order LO (Γ) is good only near the gap. Away from the gap the calculated curve drops off much more sharply than the experimental points. This

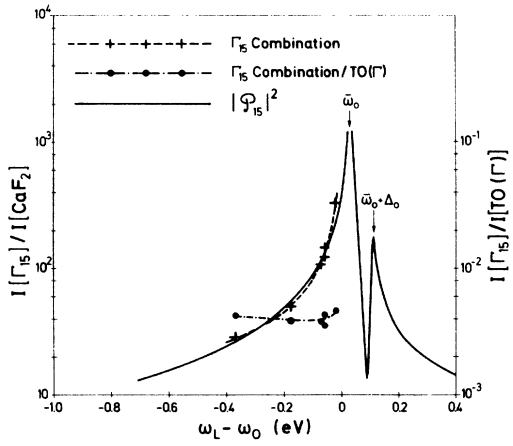

FIG. 8. Resonance of the TO-plus-LO combination peak at 755 cm^{-1} in the Γ_{15} component of the Raman spectrum in the region of the E_0, $E_0+\Delta_0$ gaps. The dots and crosses are described in Fig. 5. The solid line $|\mathcal{P}_{15}|^2$ is the same as the solid line of Fig. 3, except for a vertical shift which corresponds to a multiplicative constant.

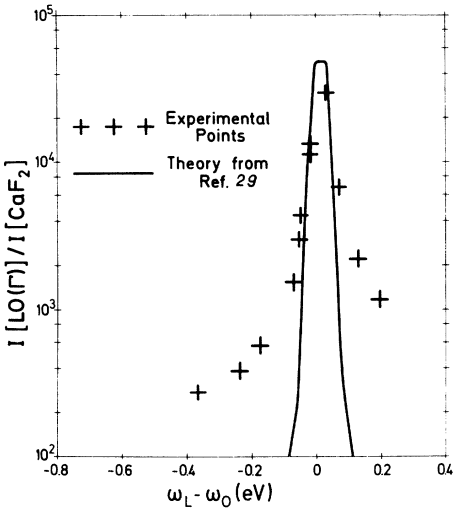

FIG. 9. Resonant behavior of the forbidden first-order LO (Γ) mode in the region of the E_0, $E_0+\Delta_0$ gaps of GaP. The E_0 gap occurs at the zero of the horizontal scale. The data are referred to 300°K, corrected for absorption, spectrometer response, etc. (see text). The theoretical calculation of Zeyher *et al.* (Ref. 29, solid line) was fitted to our experimental points (crosses) by means of a multiplicative constant (vertical shift).

disagreement can be interpreted as due to the presence of residual allowed LO (Γ) scattering which could arise from small errors in crystal and polarizer orientation, and from etch pits and unevenness at the surface. Because of the strength of the allowed scattering, an allowed component of only a few percent would be appreciable away from the gap. Thus, the first-order LO (Γ) peak seems to be produced by admixture of allowed and forbidden scattering, dominated by the forbidden component near the resonant gap.

Figure 10 shows the resonance of the combination excitation consisting of TO-plus-LO (Γ) phonons occurring in the Γ_{15} component of the scattering. The tensor symmetry of this peak was determined from separate measurements for various polarization configurations at room temperature with 4416-Å exciting light. The TO-plus-LO (Γ) peak is not present for exciting photon energies away from the gap, but first emerges from the background approximately at $\omega_L - \omega_0 = -0.07$ eV and then undergoes an enhancement of two orders of magnitude. Above the gap the peak quickly decreases and disappears into the background. The agreement between the experiment and the forbidden-LO curve of Zeyher *et al.*[29] is very good, thus suggesting some relationship between these two processes.

The two-LO (Γ) overtone mode shown in Fig. 11 undergoes a resonance enhancement of nearly four orders of magnitude. It emerges from the shoulder at the high-frequency cutoff of the second-order spectrum, where the density of states is approaching zero. The same theoretical curve for forbidden LO scattering also represents very well the two-LO (Γ) measurements for reasons which will be dis-

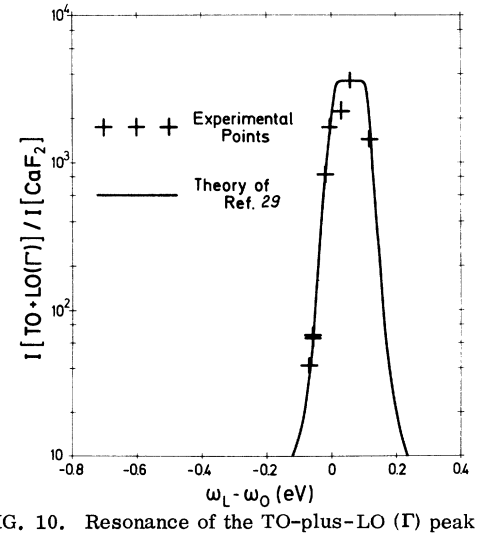

FIG. 10. Resonance of the TO-plus-LO (Γ) peak which appears in the immediate vicinity of the E_0 gap. The data were corrected and the theoretical curve of Ref. 29 fitted to our data as in Fig. 9.

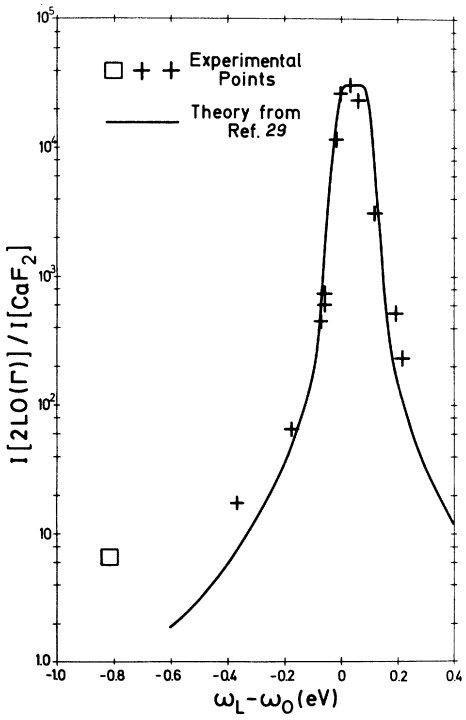

FIG. 11. Resonance of the two-LO (Γ) mode in GaP in the region of the E_0, $E_0+\Delta_0$ gaps. The data were corrected as in Figs. 9 and 10. The square represents a data point from Ref. 39. The theoretical curve of Ref. 29 was fitted to the data as in Figs. 9 and 10.

cussed in Sec. V. The slight discrepancy away from the gap can again be attributed to a background.

V. DISCUSSION

The various features observed in the Raman spectra of GaP exhibit well-defined selection rules: For instance, the Γ_1 spectrum is dominated by overtones while the Γ_{15} spectrum exhibits mainly combinations, the strongest being the LO-TO structure. These selection rules follow from the rigid-ion model of Eq. (20) under the assumption of two equal atoms per unit cell (germanium). Apparently GaP is sufficiently similar to a group-IV material that the selection rules hold (the *electronic* structure of GaP is indeed very close to the *average* of germanium and silicon; nevertheless, the vibronic structure is quite different because of the different atomic masses of Ga and P). According to Eq. (24), however, scattering by two TO phonons with orthogonal polarizations should also appear in the Γ_{15} spectrum with a strength similar to that of the LO-TO spectrum. This conclusion does not agree with our experimental observation: The Γ_{15} spectrum of Fig. 2 shows negligible TO-TO scattering.

The one-phonon TO (Γ) spectrum has Γ_{15} symmetry, as expected: The signal observed for the Γ_1 and Γ_{12} components ($\Gamma_1+4\Gamma_{12}$ experimental configuration) is very small ($\frac{1}{25}$ of the allowed Γ_{15} signal) and can be dismissed as residual owing to misorientations and surface conditions. The forbidden LO scattering, on the contrary, becomes near resonance almost as strong as the allowed TO (see Fig. 9) provided we observe it with parallel polarizer and analyzer. With crossed polarizers the forbidden LO signal becomes 50 times smaller. This result agrees with any of the theoretical calculations of Fröhlich-interaction-induced forbidden LO scattering.[26-30] The strongly resonant two-LO ($\sim\Gamma$) scattering has Γ_1 symmetry; it is thus also only seen for the parallel-parallel polarization configuration, in agreement with the mechanism proposed in Sec. II. As discussed in that section, the two-LO (Γ) scattering is due to the Fröhlich interaction of each of the participating phonons with the electronic states. The agreement between the observed line shape and the calculation of Zeyher *et al.*[29] (Fig. 11) confirms this assignment. Deviations from the theoretical curve away from the gap are to be attributed either to a nondispersive background in the Raman tensor or to the large experimental error when the resonant two-LO (Γ) structure nearly disappears under the general two-phonon scattering. Similar background, this time larger because of the relatively strong residual allowed component, also appears for the one-LO-phonon scattering in Fig. 9.

The TO-plus-LO (Γ) scattering of Fig. 10 only appears in the Γ_{15} component. We are, at present, not able to understand in detail the nature of this scattering mechanism. It may be Fröhlich-interaction-induced LO and deformation-potential TO scattering. Such a process would not be forbidden since the Fröhlich part is proportional to k_1^2, instead of q^2 like in Eq. (28). The other alternative is a double first-order deformation-potential process which, if of the form of Fig. 1(b), would have the observed resonance behavior, $(\omega-\bar{\omega}_0)^{-3}$. One may rule out such a process since a similar TO-TO process is not observed. It is, however, interesting to point out that the TO-TO processes with phonons at general points of the Brillouin zone are not observed in the Γ_{15} spectrum either, a fact that casts some doubt on the argument given above.

All of the mechanisms just described for the processes involving two phonons near Γ require a cutoff mechanism to limit the $\vec{k}$ of the phonons to points near Γ. In the case of the exciton-Fröhlich interaction, the phonon wavelength must be larger than twice the Bohr radius of the exciton. For GaP this Bohr radius is 56 Å,[36] and thus $\vec{k}$ is limited to values of the order of 0.03 a.u., corresponding to $\frac{1}{20}$ of the "radius" of the Brillouin zone. We also find another cutoff mechanism in the fact that as $\vec{k}$ increases one of the three resonant energy denominators of process (b) becomes nonresonant since the intermediate state moves away from the zone edge. Taking the resonance width from Figs. 9–11 as ~ 0.1 eV, a reasonable cutoff would take place for an energy denominator ~ 1 eV (resonance down by a factor of 10). For a mass of $\sim 0.2 m_0$[35] we find a cutoff for $\vec{k}\simeq 0.1$ a.u., still sufficiently smaller than the radius of the Brillouin zone.

We notice that Figs. 5–7 show the theoretically predicted spin-orbit structure. The structure at $\bar{\omega}_0+\Delta_0$, clear for the TA scattering of Fig. 5, only appears as a shoulder in Figs. 6 and 7, a fact attributable in part to the lifetime broadening that results from having measured these points at high temperature. [The $\bar{\omega}_0-\bar{\omega}_0+\Delta_0$ structure is particularly clear in the $I(2\mathrm{TO}(L))/I(\mathrm{TO}(\Gamma))$ ratio.] We should keep in mind, however, that the quasistatic approximation ($\Omega_1+\Omega_2=0$) holds well for Fig. 5 but runs into problems in the cases of Figs. 6 and 7 ($\Omega_1+\Omega_2\simeq\Delta_0$).

Also, the two-TA data (Fig. 5) reach at the $E_0-E_0+\Delta_0$ peaks values considerably lower than the theoretical ones (this fact is not as serious in Figs. 6 and 7). One can speculate that a strongly resonant component of the Raman tensor, of type (b) (Fig. 1) and of opposite sign to the type-(a) component given by the solid line of Fig. 5, reduces the strength of the resonance near the peaks. The two-TA ($X\rightarrow K$) phonon peak is particularly apt to show such type-(b) resonance with three equal energy denominators: The conduction bands of GaP have

an X minimum below the Γ_1 minimum and a K point nearly degenerate with Γ_1.[37,38] The X and K phonons connect the Γ_1 point of the conduction band with points at the edge of the zone of nearly the same energy. Thus, strongly resonant type-(b) processes are expected to take place.

These processes may be particularly important for the two-TA scattering because the corresponding type-(a) processes are rather weak. Figure 5 seems to indicate a scattering strength of the same order as Figs. 6 and 7. We must, however, keep in mind that these figures have been refered to room temperature, at which the Bose–Einstein excitation factors for the TO phonons are approximately 1, but the factors for the TA phonons are much larger (~2.5). Also, the factor of $1/\Omega$ in Eq. (6) makes two-TA stronger than two-TO scattering. Thus, everything else (i.e., the deformation potentials) being equal the two-TA scattering should be much stronger than the two-TO. Figures 5–7 show that this is not the case. This fact can be seen more clearly in the values of the two-phonon deformation potentials D_1 and D_{15} obtained from the ratios of the integrated intensities of the two-TA, two-TO, two-LO, and LO-plus-TO spectra to that of the one-TO peak. These ratios and the corresponding deformation potentials found with Eqs. (6), (11), (16), (18), (22), and (24) are listed in Table I. The deformation potentials D_1 and D_{15} are two orders of magnitude smaller than those calculated with pseudo-wave-functions in Sec. II.

TABLE I. Experimental ratios of areas under second-order Raman features to area under first-order TO peak $\{I(\text{mode})/I(\text{TO}(\Gamma))\}$. Also, corresponding ratios of phonon-induced energy shifts $(\delta^{(2)}\omega_0/\delta^{(1)}\omega_0)$ and electron–two-phonon deformation potentials (D). An uncertainty of about 30% is expected for these numbers.

Mode	two TA	two TO	two LO	TO plus LO
$\frac{I(\text{mode})}{I(\text{TO}(\Gamma))}$	0.160	0.050	0.035	0.015
$\frac{\delta_1^{(2)}\omega_0}{\delta^{(1)}\omega_0}$	1.5×10^8	3.8×10^8	5.0×10^8	...
$\frac{\delta_{15}^{(2)}\omega_0}{\delta^{(1)}\omega_0}$	...	...	...	5.4×10^8
D_1 (eV)	390	965	1260	...
D_{15} (eV)	...	...	...	450

ACKNOWLEDGMENTS

We would like to thank Professor Heywang of Siemens for supplying the GaP sample used in this experiment, Dr. R. Zeyher and Dr. K. L. Ngai for making available their calculations prior to publication, and Dr. T. P. Martin for a critical reading of the manuscript.

*On leave from Brown University, Providence, R. I.; Address after 1 September 1973: National Bureau of Standards, Institute for Materials Research, Washington, D. C.

[1] A. D. Bruce and R. A. Cowley, J. Phys. C **5**, 595 (1972).

[2] R. Haberkorn, M. Buchanan, and H. Bilz, Solid State Commun. **12**, 681 (1973).

[3] M. Krauzman, in *Light Scattering Spectra of Solids*, edited by G. B. Wright (Springer-Verlag, New York, 1969), p. 109.

[4] K. H. Rieder, B. A. Weinstein, M. Cardona, and H. Bilz, Phys. Rev. B (to be published).

[5] B. A. Weinstein and M. Cardona, Solid State Commun. **10**, 961 (1972); Phys. Rev. B **7**, 2545 (1973).

[6] K. Uchinokura, T. Sekine, and E. Matsuura, Solid State Commun. **11**, 47 (1972).

[7] P. A. Temple and C. E. Hathaway, Phys. Rev. B **7**, 3685 (1973).

[8] B. A. Weinstein, J. B. Renucci, and M. Cardona, Solid State Commun. **12**, 473 (1973).

[9] M. P. Fontana and E. Mulazzi, Phys. Rev. Lett. **25**, 1102 (1970).

[10] J. F. Scott, T. C. Damen, W. T. Silfvast, R. C. C. Leite, and L. E. Cheesman, Opt. Commun. **1**, 397 (1970).

[11] J. F. Scott, R. C. C. Leite, and T. C. Damen, Phys. Rev. **188**, 1285 (1969).

[12] J. F. Scott, T. C. Damen, R. C. C. Leite, and W. T. Silfvast, Solid State Commun. **7**, 953 (1969).

[13] K. Ganguly and J. L. Birman, Phys. Rev. **162**, 806 (1967).

[14] M. Cardona, in *Proceedings of the Enrico Fermi Summer School*, Varenna, 1971 (Academic, New York, 1972).

[15] A. Pinczuk and E. Burstein, in *Proceedings of the Tenth International Conference on the Physics of Semiconductors, Cambridge, Mass.*, 1970 (U.S. AEC, Tech. Infor. Div., Oak Ridge, Tenn. 1970), p. 727.

[16] L. R. Swanson and A. A. Maradudin, Solid State Commun. **8**, 859 (1970).

[17] M. Cardona, Solid State Commun. **9**, 819 (1971).

[18] R. Loudon, Adv. Phys. **13**, 423 (1964).

[19] See, for instance, A. S. Davydov, in *Quantum Mechanics*, edited by D. TerHaar (Pergamon, Oxford, England, 1965), p. 560.

[20] M. Cardona, *Modulation Spectroscopy* (Academic, New York, 1969).

[21] F. Cerdeira and M. Cardona, Phys. Rev. B **5**, 1440 (1972).

[22] A. I. Ansel'm and I. G. Lang, Fiz. Tverd. Tela **1**, 683 (1959) [Sov. Phys.-Solid State **1**, 621 (1959)].

[23] P. J. Lin-Chung and K. L. Ngai, Phys. Rev. Lett. **29**, 1610 (1972); K. L. Ngai and E. J. Johnson, Phys. Rev. Lett. **29**, 1607 (1972).

[24] F. Herman and S. Skillman, *Atomic Structure Calculations*, (Prentice-Hall, Englewood Cliffs, N. J., 1963).

[25] C. Herring, in *Proceedings of the International Conference on the Physics of Semiconductors, Prague, 1960* (Academic, New York, 1961), p. 60.

[26] R. Martin, Phys. Rev. B **4**, 3676 (1971).

[27] J. G. Gay, J. D. Dow, E. Burstein, and A. Pinczuk, in *Light Scattering in Solids*, edited by M. Balkanski (Flammarion, Paris, 1971), p. 33.

[28] B. Bendow, J. L. Birman, A. K. Ganguly, T. C. Damen, R. C. C. Leite, and J. F. Scott, Opt. Commun. **1**, 267 (1970).

[29] R. Zeyher, C. S. Ting, and J. L. Birman (unpublished).

[30] R. M. Martin and T. C. Damen, Phys. Rev. Lett. **26**, 86 (1971).

[31]A. Pinczuk and E. Burstein, Phys. Rev. Lett. **21,** 1073 (1968).

[32]P. J. Dean, G. Kaminsky, and R. B. Zetterstrom, J. Appl. Phys. **38,** 3551 (1967).

[33]V. K. Subashiev and G. A. Chalikyan, Phys. Status Solidi **13,** K91 (1966).

[34]R. A. Loudon, J. Phys. (Paris) **26,** 677 (1965).

[35]W. Dreybrodt, W. Richter, and M. Cardona, Solid State Commun. **11,** 1127 (1972).

[36]D. D. Sell and P. Lawaetz, Phys. Rev. Lett. **26,** 311 (1971).

[37]M. L. Cohen and T. K. Berstresser, Phys. Rev. **141,** 789 (1966).

[38]F. H. Pollak, C. W. Higginbotham, and M. Cardona, J. Phys. Soc. Jap. Suppl. **21,** 20 (1966).

[39]S. Fray, F. A. Johnson, R. Jones, S. Kay, C. J. Oliver, E. R. Pike, J. Russell, C. Sennett, J. O'Shaughnessy, and C. Smith, in Ref. 3, p. 139.